reduces the projectile wave functions in the nuclear interior compared to those for "equivalent" local potentials. A simple nonlocality correction factor may be applied to the wave function generated by the local potentials.[39] In the cluster transfer calculations a similar radial correction factor may routinely be used in zero-range calculations to compensate for finite range effects,[39,40] instead of the more time-consuming exact finite range calculation[31] that we made for a few cases. If the inclusion of these improvements and refinements in (d,Li^6) calculations should lead to even better agreement with experiment one ought to feel quite confident that the single-step cluster transfer model is sufficiently realistic to be used in the analysis of (d,Li^6) data. We realize that our present calculations do not even exhaust all effects that direct interaction theory in general recognizes as important. In particular, recoil and exchange terms may be quite important for our light targets. Nevertheless, it is felt that the present simple reaction model has been surprisingly successful, and may be even more useful for higher energies and heavier targets.

Keeping in mind our qualified acceptance of the proposed (d,Li^6) reaction mechanism we again refer to the spectroscopic information contained in Table II. There is no doubt that a drastic difference exists for α pickup from p shell and the light s,d shell nuclei. The deducible α parentages for the target ground states agree, at least qualitatively, with simple shell-model expectations.[36,11] The dominance of simple shell-model configurations is also indicated by the quite comparable probability for 5-nucleon transfer reactions observed in the s,d shell nuclei.[23,41]

[39] J. K. Dickens and F. G. Perey, Oak Ridge National Laboratory Report No. ORNL-3858, 1965 (unpublished).
[40] J. K. Dickens, R. M. Drisko, F. G. Perey, and G. R. Satchler, Phys. Letters **15**, 337 (1965).
[41] L. J. Denes and W. W. Daehnick (to be published).

PHYSICAL REVIEW VOLUME 148, NUMBER 3 19 AUGUST 1966

Elastic and Inelastic Electron Scattering from C^{12} and O^{16}†

HALL CRANNELL
High Energy Physics Laboratory, Stanford University, Stanford, California
(Received 3 March 1966)

Elastic and inelastic electron scattering from C^{12} and O^{16} has been studied for various scattered electron angles, using primary beam energies from 600 to 800 MeV. These studies cover a range of the square of the momentum transferred to the nucleus of 2.79 to 11.45 F^{-2} for C^{12}, and 2.79 to 8.52 F^{-2} for O^{16}. A procedure for subtracting the effects of energy loss due to radiation of the electrons is developed. With the resolution obtained in this experiment it is possible to resolve elastically scattered electrons from inelastically scattered electrons. In many instances it is also possible to resolve electrons which have excited discrete nuclear levels in C^{12} and O^{16}. Inelastic electron scattering due to excitation of nuclear levels is observed for the 4.43-MeV 2^+ and 9.6-MeV 3^- levels in C^{12}, and for the 6.1-MeV levels in O^{16}. Differential cross sections for excitation of these levels as well as for elastic scattering are determined. Absolute values of the cross sections are obtained by comparison with known absolute proton cross sections. Analysis of the data using the first Born approximation shows that the root-mean-square radii of C^{12} and O^{16} are 2.40±0.02 F and 2.65±0.04 F, respectively.

I. INTRODUCTION

THE advent of high-energy electron accelerators has facilitated experimentation aimed at gaining more detailed knowledge about the electromagnetic charge distributions of nuclei. These experiments have consisted of scattering high-energy electrons from target nuclei and studying the energy and angular distribution of the scattered electrons.[1] This investigation[2] involved a study of elastic and inelastic electron scattering from two nuclei, C^{12} and O^{16}. Both of these nuclei have already been the subject of investigation by several experimenters.[3–6] Because these nuclei have been studied so extensively in the past, it is interesting to consider the factors that motivated additional experimental work at this time.

The most sensitive region of electron-scattering measurements of nuclear characteristics is near a diffraction minimum in the cross section. The most successful model to date for P-shell nuclei, the harmonic-well shell model, predicts only one diffraction minimum

† Work supported in part by the U. S. Office of Naval Research, Contract [Nonr 225(67)].
[1] A general review has been given by R. Hofstadter, Ann. Rev. Nucl. Sci. **7**, 231 (1957).
[2] A more detailed description of this experiment is given in the author's Ph.D. thesis, Stanford University, 1964 (unpublished).
[3] J. H. Fregeau, Ph.D. thesis, Stanford University, 1956 (unpublished).
[4] J. H. Fregeau and R. Hofstadter, Phys. Rev. **99**, 1503 (1955).
[5] H. F. Ehrenberg, R. Hofstadter, U. Meyer-Berkhout, D. G. Ravenhall, and S. E. Sobottka, Phys. Rev. **113**, 666 (1959).
[6] U. Meyer-Berkhout, K. W. Ford, and A. E. S. Green, Ann. Phys. **8** (N. Y.), 119 (1959).

in the elastic cross section, while some other models[6] predict a second diffraction minimum within the momentum-transfer range of this investigation. Hence, the presence, or lack, of a second diffraction minimum would decide between possible models for the ground-state nuclear charge density.

In much the same way that elastic electron scattering is a method of investigating the ground state of a nucleus, inelastic electron scattering provides a method of studying certain excited nuclear states. Therefore, the same motivations apply to inelastic scattering from nuclear levels as to elastic scattering. An extended range of measurement would help to select the correct model of the excited nucleus. In addition, with the method of acquiring data employed in this experiment, data for the inelastic levels were obtained at the same time as the data for elastic scattering. Hence little additional experimental time was required to obtain the inelastic data.

Except for regions near a diffraction minimum, the scattering cross section diminishes rapidly as a function of q (q is the four-momentum transferred to the nucleus). For this reason there is a practical limit to the maximum transfer that can be studied with any given experimental situation. Such a practical limit had been approached by Ehrenberg *et al.*[5] However, several experimental improvements have taken place recently which made further study possible. First, the maximum incident-electron energy attainable from the Mark III linear accelerator increased from 700 MeV to more than 1200 MeV. (For a constant momentum transfer the cross section increases with increasing energy.) Secondly, the incident beam intensity has been increased by approximately a factor of 10. Thirdly, a new larger spectrometer was installed. This spectrometer has a solid angle larger by a factor of 2, and better intrinsic resolution than the spectrometer used by Ehrenberg *et al.* Fourthly, a system of 10 counters was used with the spectrometer. These counters were arranged in such a manner that the advantage of good resolution obtained by a small counter and the advantage of the high counting rate obtained by a large counter were realized simultaneously.

Several factors influenced the choice of C^{12} and O^{16} as targets for this experiment. As in all even-even nuclei, the ground states have zero spin and no magnetic moment. Since both are closed-shell light nuclei, they are relatively simple to analyze theoretically. Both C^{12} and O^{16} are found abundantly, and are easy to obtain as target materials.

Extensive investigations of these nuclei by other experimental methods have revealed many excited states, or nuclear levels. However, the lowest excited states are sufficiently separated from the ground state so that the lowest levels can be easily resolved from the ground state in electron scattering experiments. This separation allowed an independent investigation of those levels.

II. EXPERIMENTAL APPARATUS

A beam of electrons of the desired energy was obtained from the linear electron accelerator. The experimental apparatus used for determining cross sections was very similar to that described by earlier workers.[4] The energy of the electrons was analyzed by a system of bending magnets. The desired energy spread in the incident beam of electrons was chosen by adjusting the width of the energy-defining slits. These slits were adjusted to allow $\frac{1}{3}\%$ spread in the beam for most of the experiment. For measurement of the smallest cross sections, the slits were opened to allow an energy spread of $\frac{1}{2}\%$ in the incident beam, in order to gain beam intensity.

The magnetic field in the deflecting magnet was monitored by a rotating-coil system designed by Bumiller.[7] The scattered electrons were momentum analyzed with a 183-cm, 180°, double-focusing spectrometer described by Hofstadter *et al.*[8]

Part of the electron-detection system used in this experiment was a 10-channel detector built by Croissiaux.[8] The detectors were plastic scintillators placed in a nonoverlapping pattern along the theoretical image plane at the exit of the 183-cm spectrometer. To reduce the background rate for counting electrons, a coincidence was required between one of the scintillator detectors and a fluorochemical, Čerenkov backing counter. This counter was built with faces sloping so that it would fit behind the 10-channel detector. The Čerenkov counter consisted of an aluminum tank 30.5 cm tall, and 25.4 cm long in the direction of the electrons path. The inside of the tank was lined with electropolished aluminum mirrors. To reduce the high counting rate possible in such a large counter, the counter was divided into two equal halves by placing a divider made of electropolished aluminum behind the space between channels 5 and 6 of the 10-channel detector. A schematic diagram of the 10-channel detector and the backing counter is shown in Fig. 1.

Figure 2 shows a block diagram of the electronics associated with one-half of the backing counter and the channels 1 through 5. There was an identical system for the other half of the backing counter and channels 6 through 10.

The pulses from each of the 10 scintillation detectors were sent to a discriminator circuit which rejected pulses due to low-energy background. Pulses from the discriminator were shaped and supplied one input of a fast (approximately 20 nsec) coincidence circuit. The output of the Čerenkov backing counter was also supplied to a discriminator-limiter circuit, the output of which was split and supplied to each of the associated

[7] F. A. Bumiller, Stanford University Internal Memorandum HEPL Report No. 257 (unpublished).

[8] R. Hofstadter, F. A. Bumiller, B. R. Chambers, and M. Croissiaux, in *Proceedings of the International Conference on Instrumentation for High-Energy Physics, Berkeley* (Interscience Publishers, Inc., New York, 1960).

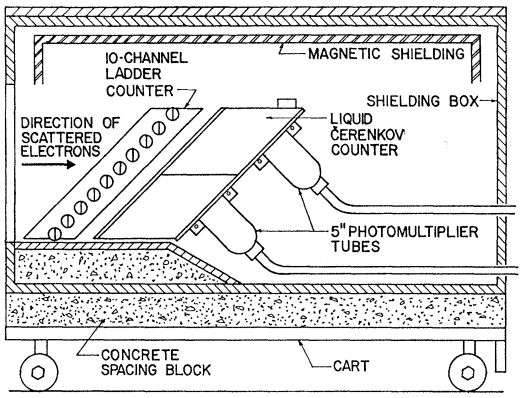

FIG. 1. A schematic view of the 10-channel detector and the liquid-filled Čerenkov counter. The entire counter assembly was surrounded with magnetic and radiation shielding, and mounted upon a movable cart so that it could be rolled into place at the exit of the spectrometer.

coincidence circuits. The output of each coincidence circuit drove a scaler which was gated by the same trigger signal as the accelerator. This system reduced the background pulse rate to a negligible level at all but the lowest cross sections, and even then the background events were not a serious problem.

Three kinds of targets were used in this experiment: two carbon targets, a water-filled target for oxygen, and a polyethylene target for electron-proton scattering normalization. The carbon targets were standard rectangular parallelepiped shapes. The oxygen target consisted of a cylinder filled with distilled water. Windows of 0.025-mm stainless steel were placed over each end of the target.

TABLE I. Target parameters.

Target	Thickness in cm	Density in g/cm³	Chemical purity	Isotopic purity
C^{12}	0.285	1.67	99.97%	98.9%
C^{12}	0.762	1.34	99.97%	98.9%
O^{16}	1.118	1.00	>99.99%	99.8%
(CH_2)	0.604	0.92	98.25%	99.98%[a]

[a] The abundance of naturally occurring H^1 in hydrogen.

In order to normalize the cross section, or to state it another way, to measure the efficiency of the counting system, electrons were scattered from a polyethylene (CH_2) target at frequent intervals during the experiment. To prevent the polyethylene target from boiling in the beam, the target, consisting of a 20-cm disk, was rotated continuously. Table I gives relevant parameters for the targets.

III. ANALYSIS OF DATA

A. Experimental Procedure

To measure correctly the energy spectrum of the scattered electrons, it was necessary to determine the relative efficiencies of the detectors. Because all channels were identical, they should ideally have had the same efficiency. In practice this was difficult to achieve because of the differences in scintillators, photomultipliers, and slight differences in the optics of the spectrometer. An improved procedure to measure the relative efficiencies of the different channels was devised.[9] A brief discussion of this method follows.

Electrons scattered from a relatively flat portion of the C^{12} inelastic continuum were detected in the 10-channel counter. In previous work,[10] the relative efficiencies were determined simply by comparing the relative counting rates. However, it was difficult to select a perfectly flat region of the inelastic continuum. Therefore, the slope of the continuum was measured by using the entire 10-detector system as a single detector. The data needed to determine the relative efficiencies were taken by setting the spectrometer momentum at several different values, spanning the region of interest. The total number of counts obtained at each momentum setting of the spectrometer was used to determine the slope of the continuum. Having determined the slope, this information was used to make a more accurate determination of the efficiencies using the observed counting rates.

The relative efficiencies of the channels could be determined to within 2% to 3% in a relatively short time. This was considered to be accurate enough, since both the C^{12} and the O^{16} cross sections (as well as the

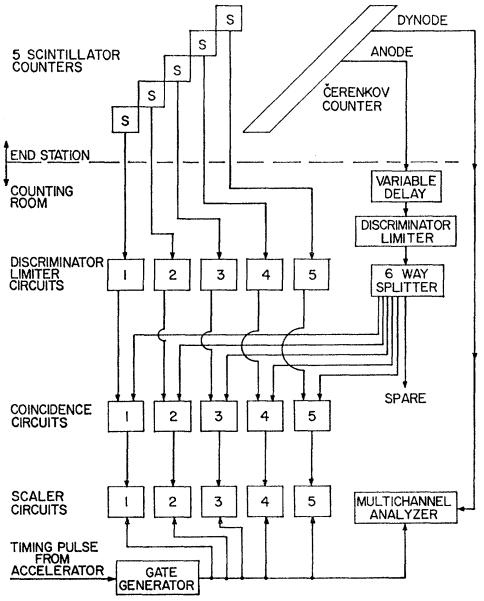

FIG. 2. Block diagram of the electronics associated with the lower half of the detector. An identical system is used for the top half of the detector.

[9] H. L. Crannell and L. Suelzle (to be published in Nucl. Instr. Methods).

[10] H. Crannell, R. Helm, H. Kendall, J. Oeser, and M. Yearian, Phys. Rev. **121**, 283 (1961).

proton normalization cross section) were taken in much the same manner, so that any error in the relative efficiencies would tend to cancel.

With an array of counters of the type used in this experiment, a large amount of data could be accumulated in a short time, so that a method of automatically reducing the raw data to cross sections was considered essential. To this end, a semiautomatic computer program to handle the data was written for Stanford's IBM 7090. The raw data were given to the computer, and the data were corrected for effects such as counting rate, counter efficiency, and for the effects of spectrometer dispersion, and then were plotted automatically.

The effects of radiative losses were also calculated, and a spectrum representing the radiation-corrected data was also plotted. While a long time was spent in developing the computer program, the analysis of data obtained subsequent to the completion of the program has been greatly facilitated.

Elastic and inelastic cross sections were obtained for C^{12} and O^{16} with incident electron energies of 600 and 800 MeV for various scattered electron angles between 32° and 60°. The range of q^2 covered for C^{12} was 2.8 to 11.45 F^{-2}, and a range from 2.8 to 8.5 F^{-2} in q^2 was covered for O^{16}. In addition to elastic cross sections, inelastic cross sections were measured for the 4.43-MeV, 2^+ and the 9.6 MeV, 3^- levels in C^{12} and for the combined levels at approximately 6.1 MeV in O^{16}. The 7.65 MeV, 0^+ level in C^{12} was not resolved at the incident-electron energies used in this experiment. This level, as well as the 4.43- and 9.6-MeV levels in C^{12} were studied at lower energies, and the lower energy results have been reported previously.[11]

For each C^{12} or O^{16} cross-section determination, a proton cross section was measured using the same incident-electron energy and scattered-electron angle. Because the absolute proton cross section was known accurately from other data, the absolute efficiency of the counter could be determined from the proton data.

The proton spectra were usually measured with four or five spectrometer settings. The spectrometer momentum settings were spaced so that the first three settings spanned the elastic peak, and the last one or two settings spanned the part of the radiative tail just below the elastic peak.

Since polyethylene (CH_2) was used as a source of target protons, it was necessary to measure the background spectrum due to the carbon. This was accomplished by scattering electrons from a carbon target matched so as to have the same number of carbon nuclei per cm^2 as the CH_2 target. A carbon spectrum was measured using the same spectrometer settings used for the CH_2 spectrum.

The spectrum of electrons scattered from C^{12} and O^{16} was usually measured with four overlapping momentum settings of the spectrometer. The counting time was adjusted so that there would be at least 200 counts in one of the channels observing the elastic peak, except at the lowest cross sections where this requirement had to be relaxed because of the finite amount of time alloted for this experiment.

[11] H. L. Crannell and T. A. Griffy, Phys. Rev. **136**, B1580 (1964).

B. Radiative Corrections

The largest corrections that must be applied to the data are the corrections due to the radiation of electrons as they traverse the target. This radiation can be divided into two principle parts: bremsstrahlung radiation due to finite target thickness, and bremsstrahlung during scattering from the nucleus. The radiation that occurs during the scattering, called Schwinger radiation, was first calculated by Schwinger,[12] and later by Suura.[13] The calculations have since been improved by Tsai,[14] and by Meister and Yennie.[15] The radiation caused by the passage of electrons through the target material is called thick target bremsstrahlung, and is roughly proportional to the thickness of the target. The theory of bremsstrahlung is discussed by Heitler,[16] and by Bethe and Ashkin.[17]

The distortion of a peak in the scattered electron spectrum, because of radiation of electrons in the target, increases the difficulty of the problem in assigning the correct area to the peak. In the case where there is a single peak or resonance in the spectrum, determining the experimental cross section involves measuring the area under the peak from the maximum scattered energy to some cutoff point (an energy interval ΔE) and using this area to determine the uncorrected differential cross section (see Ref. 14). The experimental cross section is then given by

$$(d\sigma/d\Omega)_{\text{exp}}=(d\sigma/d\Omega)_{\Delta}e^{-\delta(\Delta E)}, \tag{1}$$

where $(d\sigma/d\Omega)_{\text{exp}}$ is the experimental differential cross section, $(d\sigma/d\Omega)_{\Delta}$ is the cross section obtained by including all the area under the peak down to the cutoff, and

$$\delta(\Delta E)=\delta_s(\Delta E)+\delta_b(\Delta E), \tag{2}$$

where $\delta_s(\Delta E)$ and $\delta_b(\Delta E)$ are the terms due to Schwinger radiation and thick-target bremsstrahlung, respectively.[18]

[12] J. Schwinger, Phys. Rev. **75**, 898 (1949).
[13] H. Suura, Phys. Rev. **99**, 1020 (1955).
[14] Yung-Su Tsai, Phys. Rev. **122**, 1898 (1961).
[15] N. Meister and D. R. Yennie, Phys. Rev. **130**, 1210 (1963).
[16] W. Heitler, *Quantum Theory of Radiation* (Clarendon Press, Oxford, England, 1960), 3rd ed.
[17] H. A. Bethe and J. Ashkin, *Experimental Nuclear Physics*, edited by E. Segrè (John Wiley & Son, Inc., New York, 1953), Vol. I.
[18] The results of a recent experiment performed by A. Browman and D. Yount at Orsay, France, indicate that it is more accurate to use a correction of the form

$$(d\sigma/d\Omega)_{\text{exp}}=(d\sigma/d\Omega)_{\Delta}[1-\delta(\Delta E)].$$

Since the quantity $\delta(\Delta E)$ was small (<0.3) in this experiment, and since all cross sections (including the proton normalization cross sections) were corrected using Eq. (1), the final results of this work are not changed. The author is indebted to Dr. Yount for communication of these results prior to their publication.

Tsai shows that, when q^2 is less than the rest mass of the target nucleus Mc^2, δ_s may be written

$$\delta_s=-\frac{2\alpha}{\pi}\left\{\left[\tfrac{1}{2}\ln\left(\frac{E_0}{\eta^2\Delta E}\right)+\tfrac{1}{2}\ln\left(\frac{E_0}{\eta\Delta E}\right)-\frac{13}{12}\right]\times\left[2\ln\left(\frac{q}{mc^2}\right)-1\right]+\frac{17}{36}\right\}, \quad (3)$$

where α is the fine-structure constant, E_0 is the incident energy of the beam, mc^2 is the rest-mass energy of the electron, and η is the recoil factor and is given by

$$\eta=1+(2E_0/Mc^2)\sin^2(\theta/2), \quad (4)$$

where θ is the laboratory scattering angle, and Mc^2 is the rest-mass energy of the target nucleus.

If recoil effects are taken into consideration the term δ_b, originally suggested by Bethe and Ashkin, may be written

$$\delta_b=-\frac{t}{\ln(2)}\left\{\tfrac{1}{2}\ln\left(\frac{E_0}{\eta^2\Delta E}\right)+\tfrac{1}{2}\ln\left(\frac{E_0}{\eta\Delta E}\right)\right\}, \quad (5)$$

where t is the thickness of the target in radiation lengths. The cutoff technique described above is usually applied to hydrogen spectra with a single peak.

However, when there are excited levels in the spectrum, some of the elastically scattered electrons lose an amount of energy which causes them to be counted as inelastically scattered electrons. Separating the inelastically scattered electrons from the radiation degraded, elastically scattered electrons is necessary in order to obtain an accurate measurement of the inelastic cross section. The elastic cross section is also affected, for the size and shape of the radiative tail that is produced by the electrons that have radiated is obscured by the inelastic levels. Therefore, to obtain an accurate elastic or inelastic cross section, it is necessary to subtract the effects of the radiation. Correcting for the radiative effects will be referred to as radiative unfolding, or just unfolding.

Because average ionization losses do not affect the shape of the peaks in a spectrum, to within the resolution obtainable in this experiment, ionization losses are neglected in this treatment.

In order to correct for the effects of radiation in the measured spectrum, it is necessary to consider the shape of a spectrum due to electrons which have radiated while scattering. The shape of such a spectrum is calculated by assuming: (1) that a monoenergetic beam of electrons is incident on a target of thickness t, and that the probabilities for radiating while traversing the target and while scattering are given by Eqs. (3) and (5).

In the process of correction the experimental spectrum is divided into a number of small energy intervals. Each such interval is successively treated as the highest energy interval in the theoretical radiation spectrum. This radiation spectrum is subtracted from the experimental spectrum using an iterative numerical procedure. The resulting spectrum is then a theoretical representation of the shape that would have been measured if no radiative processes had been present.

The radiative unfolding is accomplished in the following manner. After a spectrum has been measured, and all of the simple corrections have been applied to the data points, the spectrum is divided into a number of consecutive uniform-energy intervals or bins. The electrons that are observed in the highest energy interval are electrons that did not radiate enough energy to fall outside the energy interval of the first bin. The calculated, theoretical radiation spectrum predicts the percentage of scattered electrons expected in this energy bin. The calculated spectrum also predicts the percentage of electrons to be expected in each of the lower bins due to radiative loss of energy. By subtracting this small percentage of radiation-degraded electrons associated with the first bin from each subsequent interval, the radiative effects of the first energy interval are removed. In addition, the counts remaining in the second energy interval or bin are just those that did not radiate out of the bin. The second interval can then be treated in a manner identical to the first interval. This iterative process is continued until all the intervals have been corrected.

The radiative unfolding program discussed above is used to calculate the number of electrons that would have scattered into a bin if the electrons incident on the target had not radiated. If it is assumed that the scattering cross section does not change with energy, then because of the target geometry, approximately one-half of the incident electrons that radiate do so before they scatter, and the other half radiate after they scatter.[19] However, the electrons that radiate before scattering have a lower energy than the incident beam electrons, and hence have a different cross section, or probability of scattering. This usually means that a larger percentage of the counts in the radiation tail comes from electrons that radiate before scattering.

The scattering probability for energy degraded electrons is modified by the ratio of the cross sections. This correction takes the form

$$\tfrac{1}{2}\left\{1+\left(\frac{d\sigma}{d\Omega}\right)_E\Big/\left(\frac{d\sigma}{d\Omega}\right)_{E_0}\right\},$$

where E is the energy of the degraded electron.

The validity and accuracy of the theoretical expressions used to calculate the radiative corrections are important in the final accuracy of the experimental

[19] The calculation of the radiative corrections employed here neglects the change in the bremsstrahlung and Schwinger radiation cross sections as a function of the electron energy, and neglects the effect of the electrons which radiate both before and after they scatter. This latter effect is small, and is even neglected in the original treatment, Eqs. (4) and (5).

numbers. In deriving the Schwinger radiative correction given by Eq. (4), Tsai[14] states that two conditions must be satisfied:

$$\Delta E \gg \Delta E_b/\eta^2, \quad \text{(A)}$$

$$\Delta E > [E_0^2 \sin(\tfrac{1}{2}\theta)/Mc^2]\Delta\theta, \quad \text{(B)}$$

where ΔE_b is the energy spread in the incident beam, and $\Delta\theta$ is the angular acceptance of the spectrometer. The unfolding program discussed above equates the energy interval ΔE with the bin width. In the analysis used in this experiment the bin width is typically $\frac{1}{3}$ the width of the beam energy. In this case, condition (A) is clearly violated. However, condition (A) was introduced only to assure that any interval chosen would be large enough to include all electrons that did not radiate. Since, in this experiment, a large number of bins were included in the analysis, condition (A) is in effect satisfied. Condition (B) was assumed in deriving Eq. (4) and, therefore, must be experimentally satisfied. For scattering from a heavy target such as C^{12}, condition (B) is satisfied, because the energy of the scattered electron is essentially constant, regardless of the scattering angle. However, for a lighter nucleus such as a proton, condition (B) is not necessarily satisfied.

C. Tests of the Radiative Unfolding Procedure

The radiative corrections discussed above were tested in several ways. The importance of the bin size on the correction was first checked. For this purpose a curve was visually fit to a C^{12} spectrum. This curve was then divided into bins the width of the channels. Three other bin widths were chosen: $\frac{1}{2}$, $\frac{1}{4}$, and 2 times the initial bin width. The spectrum, obtained numerically from the smooth curve, was then unfolded using each of the four bin widths. The unfolded spectra that resulted were virtually indistinguishable.

In order to check the effect of condition (B) on proton peaks, several proton peaks were unfolded using several different bin widths. Once again little if any difference was observed between the various unfolded spectra. As an additional check of the unfolding procedure, the cross sections of the unfolded proton peaks were compared with the same cross sections measured in the usual manner [choosing a cutoff energy ΔE and using Eq. (1)]. No difference greater than 2% was ever observed between the two methods.

As a check of the accuracy of the bremsstrahlung radiative corrections, cross sections were measured at the same energy and angle with two different thicknesses of carbon target. Measurements were made with both targets at 45° and 50°. No differences, larger than those expected from statistical uncertainties, were observed.

A final check on the unfolding method was to observe how well the tail due to radiative effects was calculated. This was done using several proton peaks and some of the heavier target spectra where the first excited level was well resolved. When the unfolded proton peaks were plotted with error bars, there appeared to be no remaining tail. However, when the remaining tail was analyzed by a least-squares method, it was observed that the radiative unfolding accounts for only 80% to 90% of the original tail. The same seemed to be true for the heavy-target case. The portion of the radiation tail that remains after the unfolding could be due to approximations made in the theory, or to errors in the theory, or to contamination in the target.

The unfolding method described above is satisfactory for any set of evenly spaced, nonoverlapping measurements which span the spectrum. However, when using the multichannel counter it is not always convenient to keep all the spectrometer settings evenly spaced. Moreover, to obtain the maximum possible definition with the equipment used in this experiment, several overlapping settings of the counter were used. The spectrum taken in this manner can always be

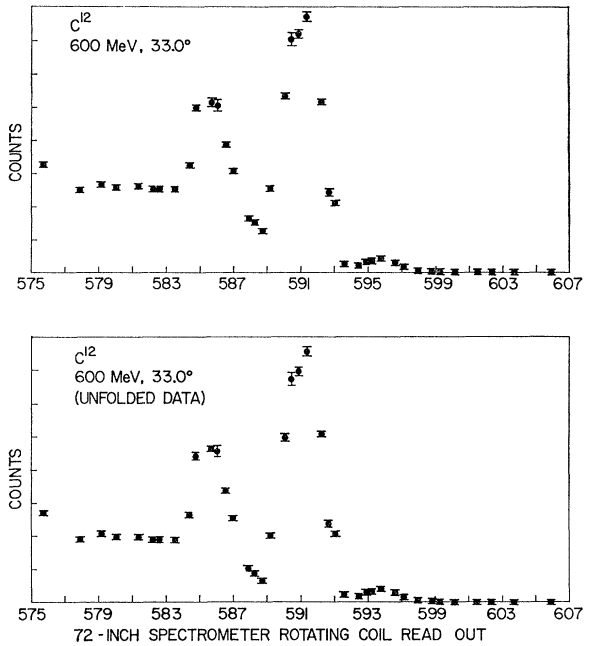

FIG. 3. Spectrum of scattered electrons at 33° from C^{12} for an incident energy of 600 MeV. Data such as this were automatically corrected and plotted as explained in the text. The abscissa gives values of the output of the rotating coil magnetic field monitor in the spectrometer. This output was adjusted to correspond closely to the scattered momentum in MeV/c. The ordinate gives the number of counts arbitrarily normalized. The errors shown with the points are statistical only. Not shown is the uncertainty in the momentum position of each point due to the uncertainty in the exact position of the scintillators and in dispersion of the spectrometer. These uncertainties amount to 0.04% of the scattered momentum. The smallest peak at the right is due to elastic scattering. The two larger peaks are due to excitation of the 4.43- and 9.61-MeV levels. In this figure and Fig. 4 the upper plot shows data points corrected for counting rate losses and for channel efficiencies. The lower plot shows the same data with the radiative effects subtracted. These corrections are discussed in the text.

[20] H. Crannell, R. Helm, H. Kendall, J. Oeser, and M. Yearian, Phys. Rev. **123**, 923 (1961).

fitted visually, and this visual fit can then be unfolded, in the manner described above. This method has been used with success in previous work.[20] It suffers from the disadvantage of creating one additional data-handling step, and from the defect of allowing a possible bias of the experimenter to influence the visual fit. For these reasons it was deemed worthwhile to develop the unfolding method further, so that the data from any arbitrary set of measurements could be handled directly.

The problems in correcting such data are twofold. First, not all portions of the spectrum are necessarily observed with the same density of measurements. Each measurement must be assigned a weight which depends on the density of measurements in the portion of the spectrum in which the measurement was made. Secondly, the measurements may overlap in an arbitrary manner.

A procedure was developed which allowed a correctly weighted average of the number of counts to be assigned to each interval or bin chosen for the radiative unfolding. The unfolding was then carried out as explained above using the calculated weighted averages.

This method of performing the radiative unfolding is straightforward, but somewhat laborious, especially if 40 or more points are taken in measuring the spectrum. An additional disadvantage is that each calculation depends on the previous one, so that any error propagates from the point where the error is made, to the end of the calculation. For these reasons, this type of calculation lends itself to the use of a computer. A program for an IBM 7090 was developed that carries out these calculations. The computer was also programmed to keep track of the statistical error as it propagated through the calculation. In addition, the computer produced a magnetic output tape containing plotting procedures. This output tape was then read by a Calcomp 665 plotter. With this plot procedure, the corrected data and then the unfolded data were plotted, and the data plots were labeled. Figures 3 and 4 show reproductions of the plots produced by this procedure.

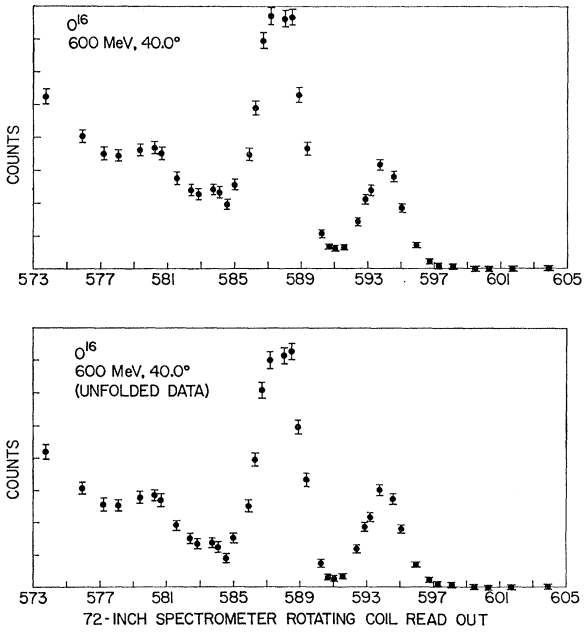

FIG. 4. Spectrum of scattered electrons at 40° from O^{16}, for an incident energy of 600 MeV. The peak due to elastic scattering and the peak due to inelastic scattering from the levels at 6.1 MeV are clearly visible. A resonance can just be observed for an excitation of approximately 14 MeV. Background due to the stainless-steel target windows has been subtracted.

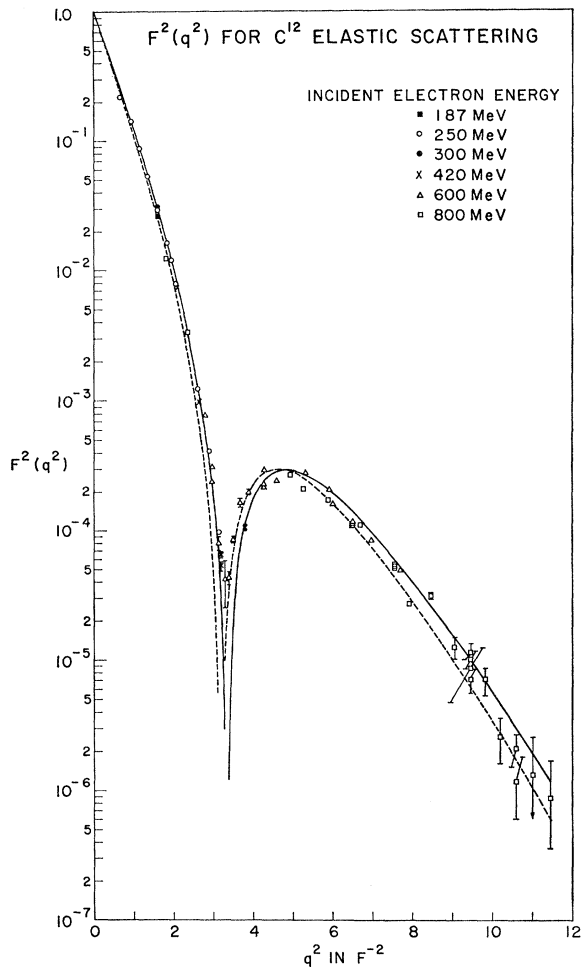

FIG. 5. $F^2(q^2)$ for elastic scattering from C^{12}. Data from earlier work have been added for comparison. The solid and dashed curves show the predictions of the harmonic-well model for two different radii. Errors shown in this figure, as well as in Figs. 6, 7, 8, and 9 are statistical only. Those points with no error bars have statistical uncertainties approximately the size of the point.

IV. RESULTS

A. Cross Sections and Form Factors

Values of the cross sections for elastic scattering and for excitation of the low-lying levels, measured in this

TABLE II. Elastic and inelastic cross sections for C^{12}.

E_0 (MeV)	θ (degrees)	Differential cross sections in cm²/sr[a] Elastic scattering	4.43-MeV level	9.64-MeV level
600	32.0	$(6.35\pm0.25)\times10^{-32}$	$(4.54\pm0.05)\times10^{-31}$	$(2.89\pm0.29)\times10^{-31}$
	33.0	$(2.35\pm0.15)\times10^{-32}$	$(3.58\pm0.05)\times10^{-31}$	$(2.09\pm0.24)\times10^{-31}$
	33.0	$(1.74\pm0.20)\times10^{-32}$	$(3.39\pm0.03)\times10^{-31}$	$(2.37\pm0.25)\times10^{-31}$
	34.0	$(5.22\pm0.64)\times10^{-33}$	$(2.50\pm0.02)\times10^{-31}$	$(1.48\pm0.15)\times10^{-31}$
	35.0	$(2.4\ \pm1.0\ )\times10^{-33}$	$(1.72\pm0.01)\times10^{-31}$	$(1.14\pm0.11)\times10^{-31}$
	35.3	$(2.40\pm0.29)\times10^{-33}$	$(1.82\pm0.01)\times10^{-31}$	
	36.0	$(4.31\pm0.24)\times10^{-33}$	$(1.30\pm0.01)\times10^{-31}$	$(9.44\pm0.95)\times10^{-32}$
	37.0	$(7.52\pm0.66)\times10^{-33}$	$(9.15\pm0.11)\times10^{-32}$	$(6.75\pm0.68)\times10^{-32}$
	38.0	$(8.14\pm0.34)\times10^{-33}$	$(5.98\pm0.09)\times10^{-32}$	$(4.49\pm0.45)\times10^{-32}$
	40.0	$(9.76\pm0.91)\times10^{-33}$	$(4.43\pm0.11)\times10^{-32}$	$(2.66\pm0.33)\times10^{-32}$
	40.0	$(7.56\pm0.24)\times10^{-33}$	$(4.48\pm0.06)\times10^{-32}$	$(4.39\pm0.44)\times10^{-32}$
	40.0	$(7.16\pm0.37)\times10^{-33}$	$(3.55\pm0.09)\times10^{-32}$	$(3.36\pm0.35)\times10^{-32}$
	41.5	$(7.00\pm0.26)\times10^{-33}$	$(1.68\pm0.05)\times10^{-32}$	$(1.66\pm0.24)\times10^{-32}$
	45.0	$(5.65\pm0.20)\times10^{-33}$	$(5.01\pm0.28)\times10^{-33}$	$(5.69\pm0.59)\times10^{-33}$
	47.5	$(3.35\pm0.11)\times10^{-33}$	$(1.68\pm0.14)\times10^{-33}$	$(2.15\pm0.72)\times10^{-33}$
	48.0	$(2.53\pm0.10)\times10^{-33}$	$(1.06\pm0.12)\times10^{-33}$	$(2.53\pm0.27)\times10^{-33}$
	50.0	$(1.46\pm0.06)\times10^{-33}$	$(4.2\ \pm1.3\ )\times10^{-34}$	$(8.4\ \pm2.1\ )\times10^{-34}$
	50.0	$(1.50\pm0.10)\times10^{-33}$	$(2.03\pm0.98)\times10^{-34}$	$(7.9\ \pm1.5\ )\times10^{-34}$
	50.0	$(1.43\pm0.03)\times10^{-33}$	$(3.99\pm0.40)\times10^{-34}$	$(1.02\pm0.10)\times10^{-33}$
	52.0	$(9.31\pm0.43)\times10^{-34}$	$(1.16\pm0.33)\times10^{-34}$	
	55.0	$(4.38\pm0.26)\times10^{-34}$	$(4.5\ \pm2.6\ )\times10^{-35}$	
	60.0	$(7.6\ \pm3.8\ )\times10^{-35}$		
800	32.0	$(1.24\pm0.08)\times10^{-32}$	$(2.12\pm0.11)\times10^{-32}$	$(1.86\pm0.19)\times10^{-33}$
	33.0	$(8.6\ \pm1.8\ )\times10^{-33}$	$(1.14\pm0.29)\times10^{-32}$	
	35.0	$(5.52\pm0.20)\times10^{-33}$	$(3.91\pm0.20)\times10^{-33}$	$(3.9\ ^{+3.9}_{-2.0}\ )\times10^{-33}$
	37.5	$(2.66\pm0.22)\times10^{-33}$	$(8.3\ \pm1.7)\ \times10^{-34}$	$(1.1\ ^{+1.1}_{-0.6}\ )\times10^{-33}$
	40.0	$(9.74\pm0.48)\times10^{-34}$	$(2.1\ \pm1.0\ )\times10^{-34}$	$(5.8\ \pm2.1\ )\times10^{-34}$
	40.0	$(9.51\pm0.62)\times10^{-34}$	$(1.99\pm0.99)\times10^{-34}$	$(5.6\ \pm1.7\ )\times10^{-34}$
	40.0	$(1.02\pm0.03)\times10^{-33}$	$(2.8\ ^{+2.8}_{-1.4}\ )\times10^{-34}$	$(8.6\ ^{+8.6}_{-4.3}\ )\times10^{-34}$
	41.0	$(4.54\pm0.12)\times10^{-34}$	$(1.12\pm0.61)\times10^{-34}$	$(2.5\ \pm1.2\ )\times10^{-34}$
	42.5	$(4.48\pm0.27)\times10^{-34}$	$(1.65\pm0.83)\times10^{-34}$	$(4.0\ \pm1.3\ )\times10^{-34}$
	44.0	$(1.56\pm0.32)\times10^{-34}$	$(6.9\ \pm3.4\ )\times10^{-35}$	$(1.0\ ^{+1.0}_{-0.5}\ )\times10^{-34}$
	45.0	$(9.9\ \pm4.9\ )\times10^{-35}$	$(9.9\ \pm4.9\ )\times10^{-35}$	$(9.9\ \pm4.9\ )\times10^{-35}$
	45.0	$(1.16\pm0.16)\times10^{-34}$	$(1.17\pm0.32)\times10^{-34}$	$(1.17\pm0.59)\times10^{-34}$
	45.0	$(1.27\pm0.17)\times10^{-34}$	$(8.7\ \pm2.0\ )\times10^{-35}$	$(1.32\pm0.68)\times10^{-34}$
	45.0	$(8.0\ \pm1.6\ )\times10^{-35}$	$(8.0\ \pm1.3\ )\times10^{-35}$	$(4.0\ \pm2.7\ )\times10^{-35}$
	46.0	$(7.4\ \pm1.8\ )\times10^{-35}$	$(7.4\ \pm1.8\ )\times10^{-35}$	$(6.4\ \pm3.2\ )\times10^{-35}$
	47.0	$(2.5\ \pm1.0\ )\times10^{-35}$	$(4.5\ \pm1.4\ )\times10^{-35}$	$(3.9\ \pm1.2\ )\times10^{-35}$
	48.0	$(1.02\pm0.51)\times10^{-35}$	$(3.58\pm0.95)\times10^{-35}$	$(1.8\ ^{+1.8}_{-0.9}\ )\times10^{-35}$
	48.0	$(1.83\pm0.54)\times10^{-35}$	$(4.30\pm0.40)\times10^{-35}$	$(4.0\ \pm2.7\ )\times10^{-35}$
	49.0	$(1.0\ ^{+1.0}_{-0.5}\ )\times10^{-35}$	$(3.2\ \pm1.7\ )\times10^{-35}$	
	50.0	$(\ <1.2\ )\times10^{-35}$	$(2.7\ \pm1.3\ )\times10^{-35}$	

[a] Errors given are those due to counting statistics only. All cross sections were measured with an angular acceptance in the horizontal plane ($\Delta\theta$) of 1.93°.

experiment, are given in Table II for C^{12} and in Table III for O^{16}. The errors given in Tables II and III arise solely from the statistical error associated with determining the area of the peak. There are other errors in determining the relative accuracy of cross sections determined from different spectra, the largest of which is a 3% statistical uncertainty in determining the efficiency of the counter. These other errors, except for a possible small error in the radiative unfolding procedure, do not affect the ratio of the inelastic and elastic cross sections determined from the same spectrum. The other errors are discussed later.

As is shown in the review paper by Hofstadter,[1] the elastic differential electron scattering cross section for spin-zero nuclei may be written in first Born approximation as

$$d\sigma/d\Omega=\sigma_{NS}[F(q^2)]^2, \tag{6}$$

where $F(q^2)$ is the form factor for elastic scattering, and where

$$\sigma_{NS}=\left(\frac{Ze^2}{2E_0}\right)^2\frac{\cos^2(\tfrac{1}{2}\theta)}{\sin^4(\tfrac{1}{2}\theta)}\frac{1}{\eta}.$$

By assuming an identical relation for inelastic electron scattering, form factors for inelastic scattering are also defined. Equation (6) presents a convenient manner in which to express the data. Since the form factors depend only on the square of the momentum transfer, the

TABLE III. Elastic and inelastic cross sections for O^{16}.

E_0 (MeV)	θ (degrees)	Differential cross section in cm²/sr[a] Elastic scattering	Inelastic scattering 6.1-MeV levels
600	32.0	$(1.38\pm0.18)\times10^{-32}$	$(7.34\pm0.07)\times10^{-31}$
	33.0	$(2.98\pm0.13)\times10^{-32}$	$(5.46\pm0.05)\times10^{-31}$
	34.0	$(3.56\pm0.15)\times10^{-32}$	$(4.08\pm0.04)\times10^{-31}$
	35.0	$(3.76\pm0.12)\times10^{-32}$	$(2.86\pm0.03)\times10^{-31}$
	36.0	$(3.65\pm0.12)\times10^{-32}$	$(2.31\pm0.03)\times10^{-31}$
	38.0	$(3.06\pm0.10)\times10^{-32}$	$(1.27\pm0.02)\times10^{-31}$
	40.0	$(2.16\pm0.06)\times10^{-32}$	$(6.16\pm0.10)\times10^{-32}$
	42.0	$(1.28\pm0.04)\times10^{-32}$	$(3.67\pm0.06)\times10^{-32}$
	44.0	$(7.58\pm0.26)\times10^{-33}$	$(1.71\pm0.04)\times10^{-32}$
	46.0	$(3.59\pm0.12)\times10^{-33}$	$(7.33\pm0.19)\times10^{-33}$
	48.0	$(1.87\pm0.06)\times10^{-33}$	$(2.91\pm0.10)\times10^{-33}$
	50.0	$(8.23\pm0.38)\times10^{-34}$	$(1.32\pm0.07)\times10^{-33}$
	52.5	$(2.61\pm0.25)\times10^{-34}$	$(4.05\pm0.38)\times10^{-34}$
	52.5	$(2.48\pm0.15)\times10^{-34}$	$(4.04\pm0.24)\times10^{-34}$
	55.0	$(6.43\pm0.69)\times10^{-35}$	$(1.30\pm0.12)\times10^{-34}$
800	32.0	$(2.10\pm0.07)\times10^{-32}$	$(4.61\pm0.13)\times10^{-32}$
	33.0	$(1.11\pm0.02)\times10^{-32}$	$(2.29\pm0.24)\times10^{-32}$
	35.0	$(5.57\pm0.16)\times10^{-33}$	$(7.57\pm0.22)\times10^{-33}$
	37.5	$(1.60\pm0.06)\times10^{-33}$	$(2.56\pm0.10)\times10^{-33}$
	40.0	$(2.27\pm0.35)\times10^{-34}$	$(3.58\pm1.12)\times10^{-34}$
	41.0	$(1.08\pm0.09)\times10^{-34}$	$(2.76\pm0.72)\times10^{-34}$
	42.5	$(5.64\pm1.34)\times10^{-35}$	$(1.9\ ^{+1.9}_{-0.8})\times10^{-34}$

[a] All cross sections were measured with an angular acceptance in the horizontal plane ($\Delta\theta$) of 1.93°. Errors given are those due to counting statistics only.

square of the form factors, $F^2(q^2)$, can be presented simply as a function of q^2.

In Fig. 5 the values of $F^2(q^2)$ measured in this experiment for elastic scattering from C^{12} are plotted.

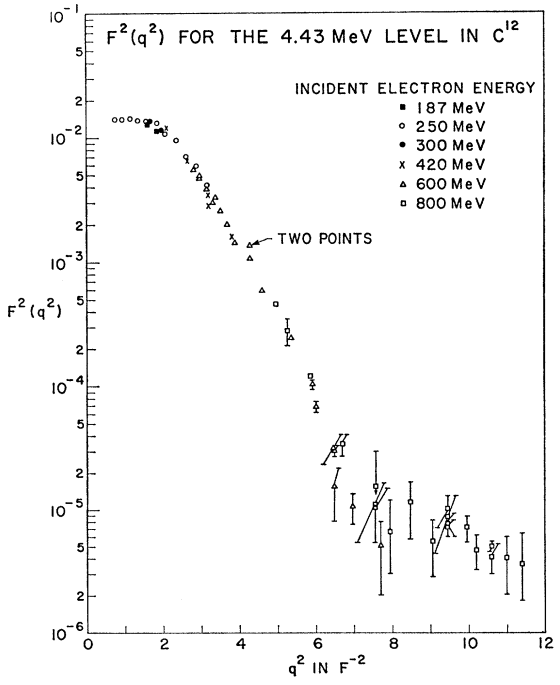

FIG. 6. $F^2(q^2)$ as a function of q^2 for the 4.43-MeV level in C^{12}. A diffraction feature can be observed at a q^2 of approximately 7 F^{-2}.

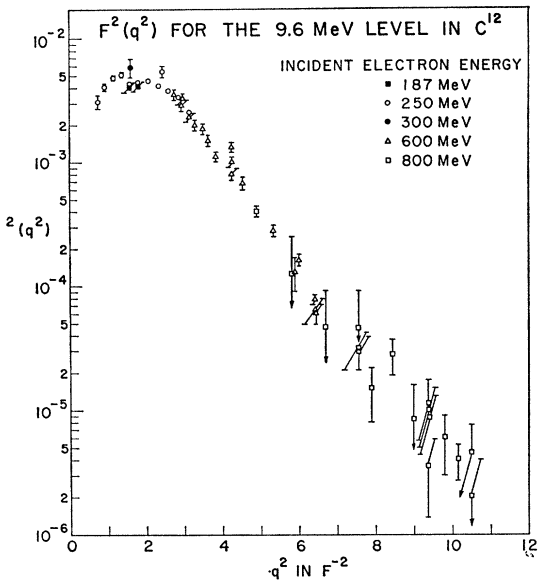

FIG. 7. $F^2(q^2)$ as a function of q^2 for the 9.6-MeV level in C^{12}.

Figures 6 and 7 present the values of $F^2(q^2)$ for the transitions to the 4.43- and the 9.6-MeV levels in C^{12}. Figure 8 presents $F^2(q^2)$ values for elastic scattering from O^{16}, and Fig. 9 is a plot of the $F^2(q^2)$ for the excitation of the set of levels at 6.1 MeV in O^{16}. The uncertainties in the plotted points in these figures represent a combination of the statistical uncertainties in determining the number of counts in the peak and in determining the efficiency of the counter. Possible systematic errors are not included.

B. Analysis of Elastic-Scattering Data

It has been shown in earlier work[6] that the simple first Born approximation is not adequate to explain the results of elastic electron scattering near the diffraction minimum, and that a more complicated phase shift analysis of the data is required to obtain a reasonable fit to the data. Phase-shift analyses have already been reported for C^{12} and O^{16}.[1] These analyses are in themselves very complicated, but are now being extended in an effort to fit the present data.[21]

The experimental data for elastic scattering from C^{12} presented in Fig. 5 show the diffraction minimum that has been seen before. Data from an earlier paper[11] are shown for completeness. The data at $q^2=11.5$ F^{-2} involve such a low cross section, and, therefore, such a large uncertainty, that it is difficult to draw any conclusion about a second diffraction minimum. No second minimum is observed at q^2 less than 11 F^{-2}.

The same statement can be made about the elastic scattering from O^{16}, although values of $F^2(q^2)$ have been measured only for values of q^2 up to 8.5 F^{-2}. As can be seen in Fig. 8, the first diffraction minimum appears

[21] R. Herman and D. G. Ravenhall (private communication).

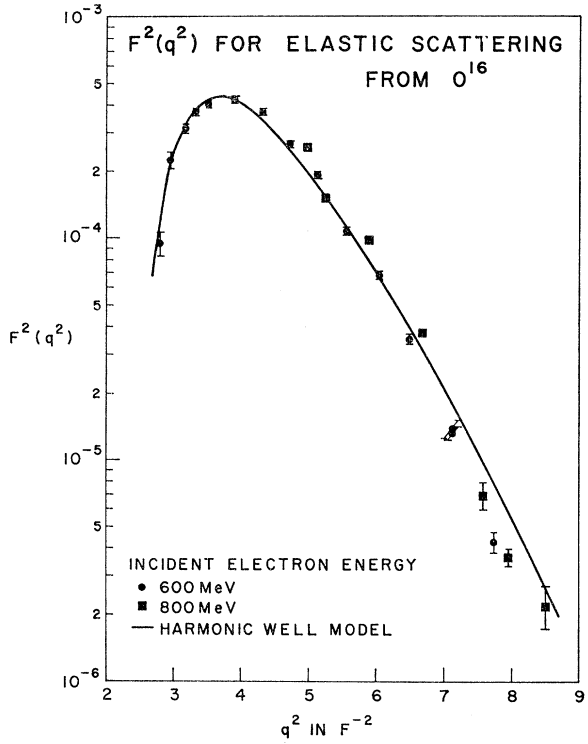

FIG. 8. $F^2(q^2)$ as a function of q^2 for elastic scattering from O^{16}. The previously observed diffraction minimum is observed at the lowest momentum transfers studied here. The curve shows the prediction of the harmonic-oscillator model with $\alpha'=1.60$ and an rms radius of 2.75 F.

near the lowest momentum transfer studied in this experiment. No second diffraction minimum is seen even at the highest momentum transfer.

Hofstadter,[1] Ehrenberg *et al.*,[5] and more recently Meyer-Berkhout, Ford, and Green[6] observed that all of the C^{12} and O^{16} cross sections measured prior to this experiment could be fit by the harmonic-well model, where the charge distribution $\rho(r)$ is given by

$$\rho(r)=\frac{2}{\pi^{3/2}}\frac{1}{B^3(2+3\alpha')}\left(1+\frac{\alpha' r^2}{B^2}\right)\exp\left(\frac{-r^2}{B^2}\right), \quad (7)$$

where $\alpha'=(Z-2)/3$, and $B=\hbar/(Mc^2\epsilon_0)^{1/2}$ (ϵ_0 is the energy interval between successive levels of the harmonic oscillator). Meyer-Berkhout *et al.* further showed that a root-mean-square (rms) radius of 2.41 F gave the best fit for C^{12}. The form factor for C^{12} ($\alpha'=4/3$) as given by first Born approximation is tabulated by Herman and Hofstadter[22] and is plotted for two values of the rms radius in Fig. 5. As can be seen, a value of 2.41 F for the rms radius fits the low-momentum-transfer data, while a rms radius of 2.47 F gives a better fit to the high-momentum-transfer points. However, Hofstadter[1] has shown that an exact phase-shift analysis gives lower values of the form factor at high momentum transfer than does the first Born approximation. Hence, at least some of the discrepancy is removed by a more accurate analysis.

A first Born approximation calculation of the harmonic-well model with $\alpha'=2$ does not give a good fit to the O^{16} cross sections measured in this experiment for any value of the rms radius. However, if α' is treated as an adjustable parameter, then a reasonably good fit is achieved with a value of $\alpha'=1.60$, and an rms radius of 2.75 F, as shown in Fig. 8. Changing the radius by 0.03 F, or the value of α' by 0.03, gives a clearly inferior fit to the data. This value of α' agrees with the value of $\alpha'=1.6$ found by Ehrenberg *et al.*,[5] and the increased accuracy of the present measurements and the extension to higher q^2 allows greater confidence in this value.

Since an accurate phase shift analysis of the data may be expected to reduce the value of the best-fit rms radius by as much as 0.05 F, a least-squares analysis of the present data was not attempted. It is hoped that

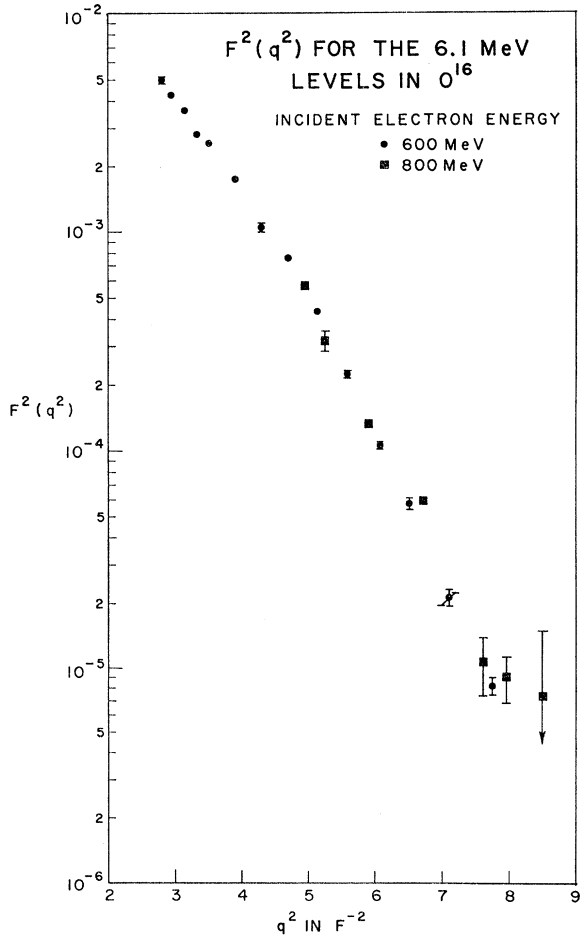

FIG. 9. $F^2(q^2)$ as a function of q^2 for the levels at approximately 6.1 MeV in O^{16}.

[22] Robert Herman and R. Hofstadter, *High Energy Scattering Tables* (Stanford University Press, Stanford, California, 1960).

an accurate phase-shift analysis may also improve the fit of the harmonic-well model at the highest momentum transfers.

The family II function for the nuclear charge distribution, suggested by Hill and Ford,[23] where the charge distribution $\rho(r)$ is given by

$$\rho(r)\sim 1-\tfrac{1}{2}\exp[-\beta(1-X)], \quad X<1,$$
$$\sim \tfrac{1}{2}\exp[-\beta(X-1)], \quad X\geq 1$$

where $X=r/r_1$ (r_1 is a parameter related to the nuclear size), and β is a surface thickness parameter, can be ruled out as a model for C^{12} by the results of this experiment. Calculations performed using values of the parameters which fit the low momentum-transfer scattering data predict a second diffraction minimum in the form factor curve at $q^2=10.5$ F^{-2}. Such a minimum is not observed.

The oscillating-drop model, suggested by Walecka,[24] also does not provide a reasonable fit to either the C^{12} or O^{16} data presented here.

C. Inelastic Scattering

Perhaps the most noticeable feature of all the inealstic scattering data is the diffraction feature in the form factor of the 4.43 MeV, 2^+ level in C^{12} (see Fig. 6). This diffraction minimum had not been observed previously.

In general, theoretical calculations of the inelastic scattering have met with less success than those for elastic scattering. A recent calculation by Gillet and Melkanoff,[25] in which they consider linear combinations of particle-hole interactions in a shell model, has been the most successful. Even so, their theoretical analysis only fits the data within experimental errors for values of q^2 up to 2 F^{-2}. No theory has yet predicted a diffraction minimum in the form factor for the excitation of the 4.43 MeV level in C^{12} near the observed momomentum transfer. Because of the number of competing, unresolved levels at approximately 6.1 MeV in the spectrum of electrons scattered from O^{16}, no attempt has been made to analyze these data. These data are included only for heuristic reasons.

V. ERRORS

The errors in determing σ_{NS} come from determing the incident energy and the scattering angle. The incident energy was known absloutely to 1%. However, the reproducibility from run to run was better than this: about 0.2%. The angle of the spectrometer could easily be set to 0.1°, and the calibration has been determined to be accurate to better than 0.02°. Thus the principle uncertainty in σ_{NS} and in q^2 is produced from the uncertainty in the incident energy, and is 2.0% in the worst case.

Errors encountered in measuring the experimental cross sections may be divided into three classes. Uncertainties in determining the relative sizes of different cross sections measured from the same energy spectrum are called "comparative errors." Errors which contribute to the relative uncertainty in cross sections measured from two different spectra are called "relative errors," and errors which contribute to the uncertainty in the absolute values of the cross section are called "absolute errors." Clearly relative errors also contribute to the absolute error, and comparative errors contribute to both the relative and absolute errors.

A. Comparative Errors

Uncertainties in the number of detected electrons, and in the radiative correction produce uncertainties in the ratio of cross sections measured from the same scattering spectrum. An error in the ratio of radiative corrections must be estimated, but is hopefully less than 1%. The uncertainty in the number of counts is statistical. Uncertainties in the relative efficiency of the channels is important only if the channels are used unequally in measuring different peaks. Because each peak is measured with several different channels, uncertainties due to channel efficiencies tend to be minimized. To check the magnitude of this effect, the efficiencies of several channels were arbitrarily changed by 10%, an amount many times greater than the error in determining the relative efficiencies. Several spectra were then corrected with these wrong efficiencies. In every case the ratio of the measured cross section to the proton normalization cross section was affected very little.

B. Relative Errors

Three quantities primarily affect the relative accuracy in the cross-section determinations. These are the accuracy of integrating the beam current, statistical uncertainty in determining the efficiency of the detector system, and uncertainties in radiative corrections.

The number of electrons in the incident beam is determined by collecting the unscattered electrons in a Faraday cup, and measuring the accumulated charge with a vibrating reed electrometer. The efficiency of the Faraday cup has been measured to be better than 99.5%, and the output of the electrometer was read to an accuracy of 1 part in 300.

Target material placed in the path of the beam causes the beam to spread, due to plural and multiple scattering. As the beam spreads, a portion of it may miss the Faraday cup, causing the Faraday cup to have an apparent loss in efficiency. Because the targets are rotated to $\frac{1}{2}$ the scattering angle, and because different targets have different thicknesses, the target thickness presented to the beam is different for each cross-

[23] D. L. Hill and K. W. Ford, Phys. Rev. **94**, 1617 (1954).
[24] J. D. Walecka, Phys. Rev. **126**, 663 (1962).
[25] V. Gillet and M. A. Melkanoff, Phys. Rev. **133**, B1190 (1964).

section determination. The magnitude of the change in Faraday-cup efficiency as a function of target thickness was measured and found to be negligible for the electron energies and target angles considered here.

The efficiency of the system is in effect determined by measuring a proton cross section and comparing it with the known proton cross section. The statistics in determining the proton cross sections varied between 2% and 3%. This is the largest uncertainty in determining the relative error between cross sections measured at different times.

Because the magnitude of the radiative corrections changes only slowly with energy and angle, the relative error associated with data taken at similar energies and angles should be small. Nevertheless, it would be possible for a systematic error in the radiative corrections to cause an error in the ratio of cross sections measured at widely differing angles or energies. It is expected, however, that such an error would be much less than the statistical error associated with the large-angle cross sections.

C. Absolute Errors

Uncertainties in the properties of the targets, in the absolute proton cross sections, and in the radiative corrections, produce uncertainties in the absolute cross section. Measurements of two of the parameters associated with the targets affect the accuracy of the absolute cross sections: (1) the density and thickness, and (2) the purity of the targets. The density of the carbon and polyethylene targets, in g/cm^2, was known to 0.2%; and the density of the water (O^{16}) target was known to about 1%. The purity of the targets is given in Table I.

Clearly, the absolute accuracy of the measurements depends on the absolute accuracy of the proton cross sections. The proton cross sections were determined from the best presently available data[26,27] and are believed to be accurate to within 5%.

The error due to the radiative corrections is much harder to analyze because it depends predominantly on the accuracy of the theoretical calculations. Tsai[28] has estimated that the error in calculating δ_s may be as large δ_s^2. (However, see Ref. 18.) The tests described previously indicate that this is a pessimistic view, at least in this experiment. By considering different bin sizes, the corrections, that must be applied to each bin, change by as much as 30%, while the final integrated answer does not change within the statistics of the measurement.

Considering the various checks that have been made, it is probable that the error in the cross sections due to radiative corrections is no greater than 5% for the lowest momentum-transfer data. At the highest momentum transfer, the radiative correction is larger by approximately a factor of 2, and, therefore, the possible error in the cross section is larger. It seems unlikely that any error in the radiative correction would be important in the high-angle cross sections, considering statistical uncertainties already present.

VI. CONCLUSIONS

New experimental results have been obtained in this work. More accurate determinations of elastic cross sections have been made for C^{12} and O^{16}; and the range of q^2, for which cross sections have been determined, has been extended. While the final conclusions may be changed slightly by a projected phase-shift analysis of the data, the following observations can be made: (1) no second diffraction minimum is observed in either the C^{12} or the O^{16} elastic scattering data; (2) the harmonic-well model, which agreed with previous results also seems to give reasonable agreement with the new, higher momentum transfer data; and (3) the family II model does not seem adequate to fit the present data.

From the inelastic scattering data, new and more accurate values of inelastic cross sections have been determined. At the higher momentum transfers, a diffraction feature in the cross section for the excitation of the 4.43-MeV level in C^{12} has been observed.

ACKNOWLEDGMENTS

The author wishes to express his appreciation to Professor Robert Hofstadter, who suggested this problem, for his continued advice and assistance throughout this project. The author is grateful for many valuable discussions with Professor M. R. Yearian and Professor J. D. Walecka. Several important suggestions essential to the writing of the computer program were offered by Mrs. C. Crannell. Thanks also go to R. Parks for design and construction of the targets and much of the other equipment; to M. Ryneveld, who assisted in the preparation for each run; to S. Berezin, C. Buchanan, H. Collard, C. Crannell, E. Erickson, P. Gram, T. Janssens, S. Swanson, and A. Walker for assistance in taking the data; and to Dr. P. Wilson and the crew of the linear accelerator for maintaining and operating the accelerator.

[26] L. H. Hand, D. G. Miller, and Richard Wilson, Rev. Mod. Phys. 35, 335 (1963).
[27] T. Janssens, Ph.D. thesis, Stanford University, 1965 (unpublished). T. Janssens, E. B. Hughes, M. R. Yearian, and R. Hofstadter, Phys. Rev. 142, 922 (1966).
[28] Yung-Su Tasi (private communication).